Rearrangement of Domain Elements of the Ca-ATPase in Cardiac Sarcoplasmic Reticulum Membranes upon Phospholamban Phosphorylation†

Sewite Negash, Shaohui Huang, and Thomas C. Squier*

Biochemistry and Biophysics Section, Department of Molecular Biosciences, University of Kansas, Lawrence, Kansas 66045-2106

Received March 16, 1999; Revised Manuscript Received April 27, 1999

ABSTRACT: Phospholamban (PLB) is a major target of the β-adrenergic cascade in the heart, and functions to modulate rate-limiting conformational transitions involving the transport activity of the Ca-ATPase. To investigate structural changes within the Ca-ATPase that result from the phosphorylation of PLB by cAMP-dependent protein kinase (PKA), we have covalently bound the long-lived phosphorescent probe erythrosin isothiocyanate (Er-ITC) to cytoplasmic sequences within the Ca-ATPase. Under these labeling conditions, the Ca-ATPase remains catalytically active, indicating that observed changes in rotational dynamics reflect normal conformational transitions. Two major Er-ITC labeling sites were identified using electrospray ionization mass spectrometry (ESI-MS), corresponding to Lys^{464} and Lys^{650}, which are respectively located within the phosphorylation and nucleotide binding domains of the Ca-ATPase. Frequency-domain phosphorescence measurements of the rotational dynamics of Er-ITC bound to these cytoplasmic sequences within the Ca-ATPase permit the resolution of the dynamic structure of individual domain elements relative to the overall rotational motion of the entire Ca-ATPase polypeptide chain. We observe a significant *decrease* in the rotational dynamics of Er-ITC bound to the Ca-ATPase upon phosphorylation of PLB by PKA, as evidenced by an *increase* in the residual anisotropy. These results suggest that phosphorylation of PLB results in a structural reorientation of the phosphorylation or nucleotide binding domains with respect to the membrane normal. In contrast, calcium activation of the Ca-ATPase in the presence of dephosphorylated PLB results in no detectable change in the rotational dynamics of Er-ITC, suggesting that calcium binding and PLB phosphorylation have distinct effects on the conformation of the Ca-ATPase. We suggest that PLB functions to alter the efficiency of phosphoenyzme formation following calcium activation of the Ca-ATPase by modulating the spatial arrangement between ATP bound in the nucleotide binding domain and Asp^{351} in the phosphorylation domain.

The Ca-ATPase, a 110 kDa integral membrane protein, is responsible for the rate-limiting sequestration of calcium into the sarcoplasmic reticulum (SR)[1] lumen, leading to muscle relaxation. In the heart, the Ca-ATPase is inhibited at submicromolar calcium concentrations by phospholamban (PLB), a 52-residue membrane protein which directly interacts with the Ca-ATPase (*1*−*3*). In response to β-adrenergic stimulation, PLB is respectively phosphorylated at Ser^{16} and Thr^{17} by cAMP-dependent protein kinase and calmodulin-dependent protein kinase (*4*, *5*). Phosphorylation of PLB results in an enhanced Ca-ATPase activity and thus an increase in the rate of cardiac muscle relaxation (*6*, *7*). A site of interaction between PLB and the Ca-ATPase was initially suggested using a peptide identical in sequence to the cytoplasmic domain of PLB, which was selectively cross-linked through Lys^3 on PLB to Lys^{397} or Lys^{400} on the Ca-ATPase (*3*). These sites of interaction were subsequently confirmed using chimeras of the Ca-ATPase in which selected sequences of SERCA3, a nonmuscle isoform of the Ca-ATPase that is not regulated by PLB, were substituted for corresponding sequences in SERCA2a (*8*, *9*). Phosphorylation at Ser^{16} results in the inability to cross-link PLB to the Ca-ATPase, suggesting the spatial orientation or proximity of these sites changes in a manner that decreases their reactivity to cross-linking. These experimental results are consistent with recent measurements using spin-label EPR and fluorescence spectroscopy, which also indicate that interactions between PLB and the Ca-ATPase are altered upon PLB phosphorylation (*10*).

However, the consequences of the phosphorylation of PLB to the structure of the Ca-ATPase remain controversial (*5*). Spin-label EPR measurements indicate that PLB phosphorylation results in a 2-fold decrease in the overall rotational dynamics of the Ca-ATPase (*11*), suggesting that the phosphorylation of PLB results in enhanced interactions

† Supported by National Institutes of Health Grant GM-46837 and the American Heart Association.

* To whom correspondence should be addressed. Telephone: (785) 864-5321. E-mail: TCSQUIER@EAGLE.CC.UKANS.EDU.

[1] Abbreviations: BSA, bovine serum albumin; BAPTA, 1,2-bis(2-aminophenoxy)ethane-*N*,*N*,*N*′,*N*′-tetraacetic acid; Ca-ATPase, Ca^{2+}- and Mg^{2+}-dependent calcium pump; cAMP, adenosine 3′,5′-cyclic monophosphate; DTT, dithiothreitol; EGTA, ethylene glycol bis(β-aminoethyl ether)-*N*,*N*,*N*′,*N*′-tetraacetic acid; Er-ITC, erythrocin 5-isothiocyanate; ESI-MS, electrospray ionization mass spectrometry; FD, frequency domain; HPLC, high-performance liquid chromatography; MOPS, 3-(*N*-morpholino)propanesulfonic acid; PKA, cAMP-dependent protein kinase; PLB, phospholamban; PMSF, phenylmethanesulfonyl fluoride; SR, sarcoplasmic reticulum; $\langle\tau\rangle$, average fluorescence lifetime; ϕ, rotational correlation time.

10.1021/bi990599j CCC: $18.00 © 1999 American Chemical Society
Published on Web 05/28/1999

between individual Ca-ATPase polypeptide chains. Likewise, resonance energy transfer (RET) measurements between single chromophores bound to the Ca-ATPase (i.e., homotransfer) demonstrate that the phosphorylation of PLB results in spatial rearrangements of individual Ca-ATPase polypeptide chains with respect to each another without altering the average oligomeric size (*12*). These results are consistent with previous radiation inactivation measurements, which have shown that the Ca-ATPase exists as a dimer in native cardiac SR membranes (*13*). In contrast, previous phosphorescence anisotropy measurements report large increases in the rotational dynamics of erythrosin isothiocyanate (Er-ITC)-labeled Ca-ATPase upon PLB phosphorylation, which have been interpreted in terms of a reversible change in the oligomeric state of the Ca-ATPase between large (dodecameric) and inactive complexes and functional small (monomers and dimers) species, which are stabilized following the phosphorylation of PLB (*5*, *14*). However, the unidentified probe sites and high stoichiometries of Er-ITC used previously suggest that the observed changes in phosphorescence anisotropies may result, in part, from changes in RET between Er-ITC molecules through homotransfer as a result of changes in their spatial rearrangement, rather than as a result of changes in rotational motion, as previously described (*15*).

Therefore, to clarify the physical mechanisms underlying PLB regulation of Ca-ATPase function, we have investigated the rotational dynamics of the Ca-ATPase in cardiac SR using low Er-ITC stoichiometries and labeling conditions previously shown to result in specific labeling of the skeletal SR Ca-ATPase (*16*). Using electrospray ionization mass spectrometry (ESI-MS), we have identified two major labeling sites for Er-ITC bound to the Ca-ATPase in cardiac SR membranes, involving Lys^{464} and Lys^{650}. In the presence of dephosphorylated PLB, there are no significant changes in the rotational dynamics of the Ca-ATPase upon calcium activation. In contrast, phosphorylation of PLB results in decreased rotational mobility of Er-ITC bound to the Ca-ATPase, which is primarily the result of a significant increase in the residual anisotropy. There are no significant changes in the amplitude or rotational correlation times associated with either domain motions or the overall rotational motion of the Ca-ATPase. These results suggest that phosphorylation of PLB primarily results in a reorientation of cytoplasmic domains within the Ca-ATPase, without large changes in oligomeric states. We suggest that changes in domain interactions may be important in facilitating the cooperative calcium activation and enhancement of ATP utilization necessary for the enhanced rates of relaxation in the heart following β-adrenergic stimulation.

EXPERIMENTAL PROCEDURES

Materials. DTT and KCl were purchased from Research Organics Inc. (Cleveland, OH). Sucrose, NaCl, ammonium bicarbonate, acetonitrile, TRIS (free base), and MOPS were purchased from Fisher Scientific (Pittsburgh, PA). $CaCl_2$ standard solutions were purchased from VWR (St. Louis, MO). Molecular mass markers, Er-ITC (isomer II), β-D-(+)-glucose, ATP (disodium salt), cAMP, cAMP-dependent protein kinase, 4-vinylpyridine, A23187, EGTA, $MgCl_2$, and HPLC grade ammonium acetate were purchased from Sigma (St. Louis, MO). Sequencing grade TPCK-treated trypsin was purchased from Promega (Madison, WI). PEP (monopotassium salt) was purchased from Boehringer (Indianapolis, IN). Glucose oxidase, catalase, pyruvate kinase, lactate dehydrogenase, and lima bean trypsin inhibitor were purchased from Worthington (Freehold, NJ). BAPTA [1,2-bis(2-aminophenoxy)ethane-*N*,*N*,*N*′,*N*′-tetraacetic acid] was purchased from Molecular Probes (Eugene, OR). Cardiac SR membranes were isolated from porcine ventricles essentially as described previously (*11*), with the inclusion of 0.3 mM PMSF, 1.0 mM benzamidine, and 0.5 μM pepstatin A in the homogenization buffer [0.3 M sucrose, 10 mM imidazole hydrochloride (pH 6.9), 3 mM NaN_3, and 0.5 mM dithiothreitol]. SR membranes were stored at −70 °C. Under optimal conditions, PKA phosphorylates 8.3 ± 1.2 nmol of PLB/mg of SR protein in these cardiac SR membranes, which on the basis of quantitative immunoblotting corresponds to phosphorylation of essentially all of the PLB molecules (*11*, *17*).

Enzyme Assays. ATP hydrolytic activity was measured as previously described (*18*), using 0.05 mg of protein/mL in 25 mM MOPS (pH 7.0), 0.1 M KCl, 5 mM $MgCl_2$, 5 mM ATP, 1.0 mM EGTA, 3 μM A23187, and sufficient calcium to yield the desired free calcium concentration, which was directly measured using the calcium-sensitive fluorophore BAPTA (λ_{ex} = 299 nm; λ_{em} = 360 nm), essentially as previously described (*19*). Under these experimental conditions, we find that BAPTA has a dissociation constant of 203 ± 7 nM. To activate the cardiac SR Ca^{2+}-ATPase by cAMP-dependent protein kinase (PKA), 1.0 μM cAMP and 20 μg/mL PKA were included in the reaction medium and the mixture was incubated at 25 °C for 10 min. The protein concentration was determined using the Amido Black method (*20*).

Chemical Derivatization of the Ca-ATPase with Er-ITC. Covalent modification of the Ca-ATPase with Er-ITC involved the protocol previously described by Birmachu and co-workers (*21*), with minor modifications. Briefly, 2 mg/mL SR protein was incubated at 25 °C for 15 min with varying amounts of Er-ITC in a buffer containing 5 mM $MgCl_2$, 100 mM KCl, and 30 mM Tris (free base, pH 8.7). In some cases, 10 mM ATP was included in the labeling buffer. The labeling reaction was stopped by 5-fold dilution with ice cold buffer containing 1 mg/mL BSA, 0.3 M sucrose, and 30 mM MOPS (pH 7.0) followed by further incubation on ice for 45 min. Er-ITC-labeled SR vesicles were pelleted by centrifugation at 100000*g* for 30 min, resuspended in sucrose buffer (SB) containing 0.3 M sucrose and 20 mM MOPS (pH 7.0), pelleted again, and finally resuspended in SB. Labeling stoichiometries were quantified by measuring the absorbance spectra following solubilization in 1% SDS and 0.1 N NaOH, using the measured extinction coefficient ϵ_{536nm}(Er-ITC) of 87 800 M^{-1} cm^{-1} (*22*).

For spectroscopic measurements, SR vesicles were modified with a final probe concentration of 0.25 nmol of Er-ITC bound/mg of SR protein. Maximal phosphoenzyme levels of this preparation suggest that there is approximately 1.0 nmol of Ca-ATPase/mg of SR protein, indicating that under these labeling conditions approximately 0.25 mol of Er-ITC is bound/mol of Ca-ATPase. Phosphorescence measurements were taken in samples containing 0.2 mg/mL Er-ITC-derivatized SR vesicles suspended in 25 mM MOPS (pH 7.0), 0.1 M KCl, 5 mM $MgCl_2$, 1.0 mM EGTA, 0.3 M sucrose, and sufficient calcium to yield the indicated free calcium concentration. Prior to spectroscopic measurements, all samples were incubated for 5 min at 25 °C in the presence

of either 50 units/mL alkaline phosphatase or 80 μg/mL PKA, 1 μM cAMP, and 5 mM ATP, and oxygen was enzymatically removed to prevent the generation of reactive oxygen species that result from Er-ITC photoreactions essentially as previously described (*22*, *23*).

Visualization of the Er-ITC-Labeled Ca-ATPase. SR proteins (15 μg per lane) were separated on a 7.5% polyacrylamide SDS−PAGE gel (*24*), and fluorescence associated with Er-ITC-labeled SR proteins was visualized prior to staining the gel by exciting Er-ITC with 254 nm UV light using an MP4 camera (Polaroid Corp., Cambridge, MA) equipped with a Schott RG540 long-pass filter using an exposure time of 1−3 s. Protein bands were then visualized following staining with Coomassie Blue.

Tryptic Digestion of the Ca-ATPase. Prior to proteolytic digestion, Er-ITC-labeled SR membranes (2 mg/mL) were incubated at 50 °C for 30 min in a digestion buffer containing 1.0 M urea, 50 mM NH_4HCO_3 (pH 8.5), and 1.0 mM DTT to reduce disulfide bonds. Exhaustive tryptic digestion of the cytoplasmic portion of the Ca-ATPase was carried out by incubating the sample with 0.04 mg/mL TPCK-treated trypsin at 37 °C for 24 h. The reaction was quenched by the addition of lima bean trypsin inhibitor to give a final concentration of 0.015 mg/mL. Soluble peptides were then separated from SR membranes by centrifugation at 200000*g* for 2 h. The supernatant was purged with nitrogen for 5 min and incubated with 10 mM 4-vinylpyridine for 1.5 h at room temperature to modify cysteine residues, thus preventing the formation of disulfide cross-links between tryptic peptides.

Reversed-Phase HPLC and Electrospray Ionization Mass Spectrometry (ESI-MS). HPLC and ESI-MS were used to identify peptides generated from trypsin digestion. Prior to electrospray ionization, peptides were separated on a 1 mm inside diameter × 5 cm long C18 reversed-phase column (Zorbax SBC18, 5 μM, 300 Å, Rockland Technologies, Newport, DE) operating at 50 μL/min and involving solvents A (95% H_2O, 5% MeOH, and 0.25% formic acid) and B (95% MeOH, 5% H_2O, and 0.22% formic acid). The solvent gradient started at 5% B at 0 min, then ramped to 10% B by 10 min, 60% by 70 min, and 100% by 80 min, and finally held at 100% B for an additional 10 min. Tryptic peptides were monitored at 534 nm with a visible detector equipped with a 3 mm path length, 1.2 μL cell (model UV-VIS 200, Linear Scientific, Fremont, CA). The chromatograph (Micro-Tech Scientific, Sunnyvale, CA) utilizes $^1/_{16}$ in. OD pistons in model UP200M pumps, and the small volume chamber in the DynaPlus mixer is filled with glass beads and is fitted with a Rheodyne 8125 injector valve (Cotati, CA). Samples were eluted from the HPLC column into the ESI source using a post detector flow splitting of 8 μL/min through a 130 μm inside diameter stainless steel needle and nebulized with a coaxial gas flow of nitrogen at a rate of 10 L/h. ESI spectra were acquired on an AUTOSPEC-Q apparatus equipped with a VG Mark III ESI source (Micromass Ltd., Manchester, U.K.). The instrument was operated in positive ion mode at a 4 kV acceleration potential and with the ESI needle and counter electrode at 7.5 and 5 kV, respectively. The mass spectrometer was tuned to a resolving power of 1800 and scanned from 200 to 2500 amu at 10 s per decade while collecting data in a continuum mode. Masses were identified through the use of GPMAW software (Lighthouse Data, Aalokken 14, DK-5250 Odense SV, Denmark) in combination with a cDNA-derived amino acid sequence of the SERCA2a isoform of porcine smooth muscle Ca-ATPase (*25*).

Phosphorescence Measurements. Frequency-domain (FD) phosphorescence measurements were performed using an ISS K2 frequency-domain fluorometer (ISS Corp., Champaign, IL), essentially as previously described (*22*). Er-ITC-derivatized SR vesicles (0.2 mg/mL) were excited using approximately 1 mW of 514 nm modulated light from an argon ion laser (Coherent Corp., Palo Alto, CA), and the phosphorescence emission passed through a Schott RG697 long-pass filter placed in front of the detector. Prior to the measurement of phosphorescence, the concentration of dissolved oxygen using a 3 mL sealed cuvette was reduced enzymatically by the addition of 17 mM glucose, 3 units of glucose oxidase activity, and 30 units of catalase activity, and subsequent incubation in the dark for at least 5 min, essentially as previously described (*23*).

Analysis of Phosphorescence Intensity and Anisotropy Decays. Phosphorescence intensity decays [i.e., $I(t)$] were fit using the Globals software package (University of Illinois, Urbana, IL) to a sum of exponentials

$$I(t) = \sum_{i=1}^{n} \alpha_i e^{(-t/\tau_i)} \tag{1}$$

where α_i are the pre-exponential factors, τ_i are the excited state lifetime decay times, and n is the number of exponential components required to describe the decay. Unless otherwise indicated, data were analyzed using frequency-independent errors in the phase and modulation that were assumed to be 0.2° and 0.005, respectively. After the measurement of the intensity decay, one typically calculates the average lifetime, $\langle\tau\rangle$, which is weighted by the fractional intensities (f_i) associated with each of the pre-exponential terms, where

$$\langle\tau\rangle \equiv \frac{\sum_{i=1}^{n} \alpha_i \tau_i^2}{\sum_{i=1}^{n} \alpha_i \tau_i} = \sum_{i=1}^{n} f_i \tau_i \tag{2}$$

and $\langle\tau\rangle$ is directly related to the average time during which the fluorophore is in the excited state. The frequency-domain anisotropy decays [i.e., $r(t)$] were fit to a model involving a sum of exponentials and a residual anisotropy (r_∞)

$$r(t) = (r_o - r_\infty) \times \sum_{i=1}^{n} g_i e^{-t/\varphi_i} + r_\infty \tag{3}$$

where r_o is the limiting anisotropy in the absence of rotational diffusion, ϕ_i are the rotational correlation times, and $r_o g_i$ is the pre-exponential term relating to the amplitudes of the total anisotropy loss associated with each correlation time. Additional details are described elsewhere (*22*, *26*, *27*). In all cases, parameter values are determined by minimizing the χ_R^2 (the F statistic) which serves as a goodness-of-fit parameter that provides a quantitative comparison of the adequacy of different assumed models (*28*, *29*).

RESULTS

Functional Effects Resulting from the Covalent Attachment of Er-ITC to the Ca-ATPase. Accurate measurements of the

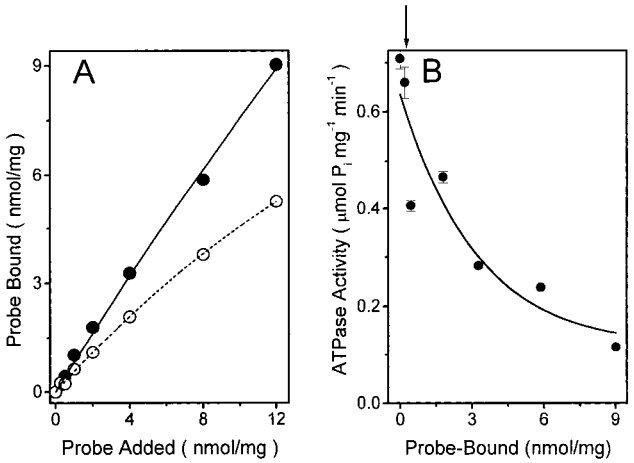

FIGURE 1: Binding and inactivation profiles for Er-ITC modification of the Ca-ATPase. Relationships are shown between labeling profiles (A) and associated loss of steady-state ATPase activity (B) due to the incorporation of various amounts of Er-ITC. Cardiac SR samples (2 mg/mL SR protein) were labeled in the presence (○) or absence (●) of 10 mM ATP in a solution containing 30 mM Tris (pH 8.7), 0.1 M KCl, and 5 mM $MgCl_2$. The arrow in panel B denotes the labeling stoichiometry used in the phosphorescence anisotropy measurements. Calcium-dependent ATPase activity was calculated as the difference between the ATPase activity measured for 0.05 mg/mL SR protein in 25 mM MOPS (pH 7.0), 0.1 M KCl, 5 mM $MgCl_2$, 5 mM ATP, 100 μM EGTA, and 3 μM A23187 in the presence of either 0.1 mM $CaCl_2$ or 0.1 mM EGTA.

dynamic structure of the Ca-ATPase using optical spectroscopy require the covalent attachment of a long-lived phosphorescent probe with a minimal loss of catalytic function. Previous measurements involving the covalent modification of the Ca-ATPase in SR vesicles isolated from skeletal muscle indicate that at low labeling stoichiometries the predominant site of modification with the phosphorescent label Er-ITC is Lys^{464}. Under these conditions, Er-ITC modification results in essentially no inhibition of ATP binding, phosphoenzyme formation, or the rate of phosphoenzyme decomposition under conditions that satisfy the high-affinity nucleotide requirement of the Ca-ATPase (*16*). Er-ITC modification blocks the secondary activation of ATPase activity normally observed in the presence of millimolar concentrations of ATP, suggesting that Er-ITC may modify a regulatory nucleotide binding site. To identify conditions that will enhance the likelihood of specific labeling of the Ca-ATPase in cardiac SR membranes by Er-ITC with minimal loss of enzymatic function, we have investigated the relationship between the extent of Er-ITC modification and enzymatic function. We observe that the presence of ATP in the labeling medium decreases the amount of Er-ITC incorporation (Figure 1A), suggesting that ATP protectable site(s) may also preferentially be modified by Er-ITC in cardiac SR membranes. Er-ITC incorporation diminishes the maximal rates of ATP hydrolysis observed in the presence of saturating ATP concentrations in a biphasic manner (Figure 1B), which is similar to that previously reported for skeletal SR membranes (*16*). However, at the same Er-ITC labeling stoichiometries, the extent of enzymatic inhibition observed in cardiac SR at saturating concentrations of ATP is approximately $^1/_2$ of that previously reported for skeletal SR membranes (*16*). Furthermore, in striking contrast to previous results obtained in skeletal SR membranes where Er-ITC modification only inhibits the catalytic activity associated with the low-affinity nucleotide requirement, the extent of inhibition of the Ca-ATPase in cardiac SR membranes is substantially larger at low (i.e., 10 μM) ATP concentrations (data now shown). These results suggest that there are differences in the specificity of Er-ITC labeling of the Ca-ATPase isoforms in skeletal and cardiac SR membranes that differentially modifies the high- and low-affinity nucleotide requirements associated with the catalytic and regulatory nucleotide binding sites.

Selective Labeling of the Ca-ATPase. To determine the specificity of Er-ITC labeling, SR proteins were separated by SDS−PAGE and the fluorescence intensity of Er-ITC was measured to identify the covalently modified protein(s). In agreement with previous studies (*21*), we find that the fluorescence intensity of Er-ITC colocalizes exclusively with the 110 kDa band on SDS−PAGE corresponding to the Ca-ATPase at both low (i.e., 0.2 nmol of Er-ITC/mg of SR protein) and higher (i.e., 2 nmol of Er-ITC/mg of SR protein) labeling stoichiometries (data not shown). These results indicate that Er-ITC selectively labels the SERCA2a isoform of the Ca-ATPase expressed in cardiac SR.

Identification of Er-ITC Labeling Sites on the Ca-ATPase. The exclusive modification of the Ca-ATPase in native cardiac SR membranes with Er-ITC ensures that phosphorescence measurements of rotational dynamics will reflect structural features of the Ca-ATPase (see below). To enhance the specificity of labeling selected sites on the Ca-ATPase and to minimize the likelihood of depolarization through homotransfer involving intra- or intermolecular resonance energy transfer (RET) between proximal Er-ITC chromophores, subsequent experiments all emphasize the covalent attachment of substoichiometric amounts of Er-ITC (i.e., 0.25 nmol/mg; Figure 1B). Under these labeling conditions, there is a 7% decrease in the maximal activity of the Ca-ATPase. Independent measurements of the abundance of the Ca-ATPase based on acid stable phosphoenzyme formation indicate the presence of approximately 1 nmol of Ca-ATPase/mg of SR protein in this preparation, suggesting that about 25% of the Ca-ATPase polypeptide chains are labeled under these conditions. Thus, the majority of Er-ITC-modified Ca-ATPase polypeptide chains remain fully functional.

Er-ITC preferentially modifies lysines located within cytosolic sequences of the Ca-ATPase, since Er-ITC is known to specifically modify lysines under these labeling conditions (i.e., pH 8.7) and essentially all the Er-ITC labels are released from the membrane pellet following exhaustive tryptic digestion and ultracentrifugation (*30*). Following incubation of these soluble peptides with 4-vinylpyridine to modify cysteine residues and prevent disulfide bond formation, the sites of Er-ITC chemical modification were identified using ESI-MS. The absorbance of the Er-ITC chromophore was monitored at 534 nm, and three chromatographic peaks were identified that contained three unique peptides whose respective masses were indicative of two unique labeling sites (i.e., Lys^{464} and Lys^{650}; Table 1). The ion currents associated with these two labeling sites are similar, suggesting that both sites are present in approximately equal amounts. These results are in contrast to previous observations in skeletal SR where Er-ITC was shown to selectively label Lys^{464} in SERCA1 and to result in the selective inhibition of the secondary activation of the Ca-ATPase

Table 1: Identification of Er-ITC-Modified CSR Ca-ATPase Tryptic Peptides by ESI-MS[a]

$[M + H^+]_{exptl}$ (Da)	$[M + H^+]_{theor}$ (Da)	peptide sequence
2699.1	2698.6	$G^{461}LS\mathbf{K}^{464}$ [b] $IERANACNSVIK^{476}$
5317.8	5319.9	$V^{437}GEATETALT\mathbf{C}$ [c] $LVEKMNVFDTELKGLS\mathbf{K}^{464}$ [b] $IERANACNSVIK^{476}$
5561.2	5561.9	$I^{638}GIFGQDEDVTS\mathbf{K}^{650}$ [b] $AFTGREFAELNPSAQREACLNARCFAR^{677}$

[a] The correspondence between resolved experimental masses and proposed peptide sequences was generated from the tryptic digestion of the Ca-ATPase. Monoisotopic masses were resolved for peptides ranging in mass from 770 to 5654 Da. Theoretical monoisotopic masses of peptides corresponding to expected tryptic fragments were calculated from the cDNA-derived sequence of SERCA2a. [b] Contains Er-ITC, which has a monoisotopic mass of 892.6 Da. [c] Cysteine modified with vinylpyridine, whose respective monoisotopic mass is 105.06 Da.

Table 2: Rotational Dynamics of Er-ITC-Labeled Ca-ATPase[a]

sample[b]	$\langle\tau\rangle$[c] (μs)	g_1	ϕ_1 (μs)	g_2	ϕ_2 (μs)	r_∞[d]
			Cardiac SR			
30 nM free calcium	310 (10)	0.59 (0.03)	7.5 (0.7)	0.23 (0.03)	600 (100)	0.06 (0.01)
0.5 μM free calcium	300 (10)	0.55 (0.03)	6.4 (0.4)	0.24 (0.03)	700 (300)	0.07 (0.01)
10 μM free calcium	280 (10)	0.60 (0.04)	7.1 (0.2)	0.21 (0.03)	500 (200)	0.06 (0.01)
0.5 μM free calcium and ATP[e]	280 (20)	0.54 (0.04)	9.0 (0.5)	0.29 (0.04)	600 (300)	0.05 (0.02)
0.5 μM free calcium, ATP, and PKA (PLB phosphorylation)	280 (10)	0.55 (0.02)	6.8 (0.4)	0.16 (0.04)	400 (100)	0.10[g] (0.01)
			Skeletal SR[f]			
10 μM free calcium	320 (60)	0.68 (0.01)	5.7 (0.5)	0.16 (0.01)	50 (10)	0.06 (0.01)

[a] Phosphorescence anisotropy decays were fit to a sum of exponentials corresponding to indicated pre-exponential amplitudes (g_i), rotational correlation times (ϕ_i), and residual anisotropies (r_∞), as described by eq 3 in Experimental Procedures. Unless otherwise indicated, values represent the average and standard errors of the mean for seven independent measurements. [b] Er-ITC-modified Ca-ATPase in native cardiac or skeletal SR membranes (0.3 mg/mL) in 25 mM MOPS (pH 7.0), 0.1 M KCl, 5 mM $MgCl_2$, 0.3 M sucrose, 1 mM EGTA, and sufficient $CaCl_2$ to yield the indicated free calcium concentration. When indicated, 5 mM ATP was added in the absence or presence of 80 μg/mL PKA and 1.0 μM cAMP. [c] Average excited-state lifetime for a four-exponential fit to phosphorescence intensity decay as described by eq 2 in Experimental Procedures. [d] $r_\infty \equiv g_3 r_o$, where $r_0 = 0.33 \pm 0.01$. [e] Indicated values represent the average and standard error of the mean for four independent measurements. [f] Data taken from ref *22*. [g] Statistical differences in mean values for cardiac SR preparations relative to values determined in the presence of 30 nM free calcium (i.e., top row) were determined using the Student's *t* test for $p = 0.05$ (*59*).

resulting from ATP occupancy of the low-affinity nucleotide binding site (*16*). However, SERCA1 contains Arg^{651} at the position homologous to Lys^{650} in SERCA2a, which would not be expected to be reactive with Er-ITC (*30*, *31*). The labeling of Lys^{650} in SERCA2a suggests that this residue is located near a nucleotide binding cleft, since erythrosin has previously been shown to preferentially partition into nucleotide binding site(s) on the Ca-ATPase (*32*, *33*). Since Er-ITC modification results in the inhibition of the high-affinity catalytic activity observed at ATP concentrations of 10 μM where the catalytic nucleotide site is selectively occupied, Lys^{650} appears to be located proximal to the high-affinity nucleotide binding site.

Measurement of Phosphorescence Lifetime and Anisotropy Decays. To identify structural differences between Ca-ATPase isoforms in skeletal and cardiac membranes, we have used FD phosphorescence spectroscopy to measure the lifetime and rotational dynamics of Er-ITC. Phosphorescence lifetime measurements will detect possible differences in the environments around Er-ITC chomophores (*34*), and are necessary for a quantitative interpretation of phosphorescence anisotropy data. The frequency response of the phosphorescence intensity of Er-ITC bound to the Ca-ATPase was measured at 20 frequencies between 0.2 and 100 kHz. Samples were treated with either alkaline phosphatase, to ensure that PLB is not phosphorylated, or PKA, to phosphorylate PLB at the indicated concentration of unbound calcium. In all cases, the intensity decay was adequately described as a sum of four exponentials, and the lifetime components are similar to previous results reported for Er-ITC bound to the Ca-ATPase in skeletal SR membranes (*22*). The average lifetime ($\langle\tau\rangle \approx 300$ μs) is not altered upon calcium activation or following phosphorylation of PLB (Table 2), indicating that the environment around Er-ITC is not affected by normal conformational changes associated with the transport activity of the Ca-ATPase.

Rotational Dynamics of the Ca-ATPase. Possible changes in the internal dynamics and hydrodynamic properties of the Ca-ATPase associated with enzyme activation were resolved using FD phosphorescence spectroscopy. The differential phase and modulated anisotropy were measured between 0.2 and 20 kHz, and in all cases can be adequately described as a sum of two exponentials and a residual anisotropy (Figure 2). This fit is superior to simpler models involving two exponentials (Figure 2D) or a single exponential and a residual anisotropy (data not shown), which are characterized by a 2-fold larger χ_R^2 and nonrandom residuals. The initial anisotropy ($r_o = 0.33 \pm 0.01$) is close to the theoretical maximum of 0.4, indicating that the majority of the phosphorescence anisotropy decay has been resolved and that Er-ITC is bound rigidly to the Ca-ATPase (*22*, *35*).

In agreement with previous results (*14*, *21*, *36*), we find that Er-ITC bound to the Ca-ATPase in cardiac SR membranes undergoes a much smaller time-dependent decrease in phosphorescence anisotropy in comparison to the Ca-ATPase expressed in skeletal SR (Figure 3). Because the angle of the transition dipoles of Er-ITC with respect to the membrane normal affects the residual anisotropy (r_∞) (*37*−*39*), observed differences in r_∞ are probably related to differences in the labeling specificity of Er-ITC for sites on the Ca-ATPase expressed in cardiac and skeletal SR membranes. One of the measured rotational correlation times for

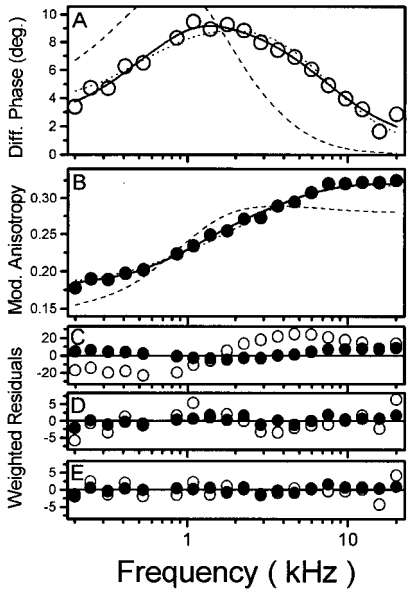

FIGURE 2: Multiexponential fits to frequency-domain phosphorescence anisotropy data. Comparison of single-exponential (- - -; $\chi_R^2 = 177$), double-exponential (•••; $\chi_R^2 = 5.5$), and three-exponential (—; $\chi_R^2 = 2.6$) fits and respective weighted residuals (C−E) to the measured differential phase (A) and modulated anisotropy (B) for Er-ITC-modified Ca-ATPase in cardiac SR. Measurements were taken using 0.2 mg/mL SR in 25 mM MOPS (pH 7.0), 0.1 M KCl, 5 mM $MgCl_2$, 0.3 M sucrose, 1 mM EGTA, and 0.6 mM $CaCl_2$; the free calcium concentration was 0.5 μM. The temperature was 25 °C. Frequency-independent errors were assumed to be 0.2° for the differential phase and 0.005 for the modulation anisotropy.

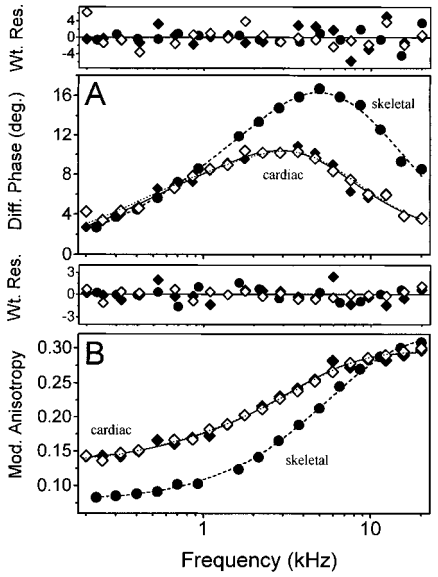

FIGURE 3: Phosphorescence anisotropy decays of cardiac and skeletal Ca-ATPase. Comparison of differential phase (A) and modulated anisotropy (B) for cardiac (◇ and ◆) or skeletal (●) SR in the presence of 30 nM (◆) or 10 μM (◆ and ●) free calcium. Lines represent the nonlinear least-squares fits to the data assuming two rotational correlation times and a residual anisotropy, as described by eq 3 in Experimental Procedures. Experimental conditions were like those described in the legend of Figure 2.

the SERCA2a isoform of the Ca-ATPase (i.e., ϕ_1) is similar to that previously measured for the SERCA1 isoform of the Ca-ATPase in skeletal SR (Table 2), which has been shown to correspond to the rotational dynamics of individual domain motions ($\phi_1 \approx 6$ μs) (*22*). However, the longer rotational correlation time observed in cardiac SR ($\phi_2 \approx 500$ μs) is

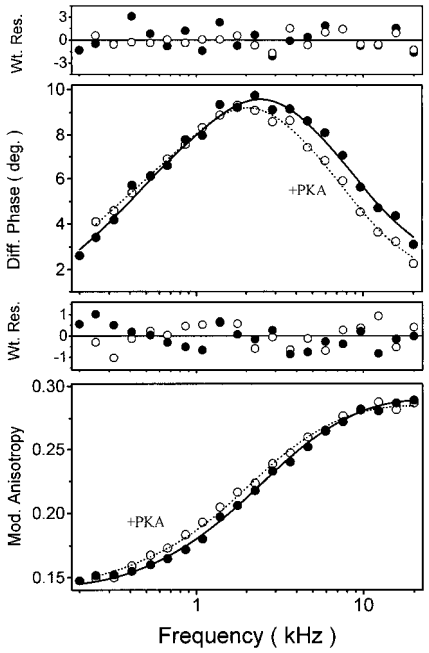

FIGURE 4: Restricted rotational dynamics of the Ca-ATPase following PLB phosphorylation. Differential phase and modulated anisotropy data and associated fits to the data for the Ca-ATPase in cardiac SR membranes in the presence of dephosphorylated PLB (●; solid line) or following PLB phospohrylation (○; dotted line), as described in Experimental Procedures. Corresponding weighted residuals are shown above the respective panels for the differential phase and modulated anisotropy. Other experimental conditions were like those described in the legend of Figure 2.

substantially greater than that observed for the Ca-ATPase in skeletal SR membranes ($\phi_2 \approx 50$ μs), which has been suggested to represent the overall rotational motion of the Ca-ATPase with respect to the membrane normal (*22*, *36*). These results are consistent with the interpretation that PLB functions to restrict the rotational dynamics of the Ca-ATPase (*11*, *14*, *21*).

Resolution of Global Structural Changes of the Ca-ATPase upon PLB Phosphorylation. The phosphorylation of PLB at Ser^{16} by PKA results in a shift in the differential phase and modulated anisotropy to lower frequencies (Figure 4), indicating that the rotational dynamics of the Ca-ATPase become slower. In contrast, no significant changes in rotational dynamics are evident upon either phosphorylation of the Ca-ATPase at Asp^{351} upon addition of ATP or following calcium activation in the presence of dephosphorylated PLB (Figure 3 and Table 2). A consideration of the fitting parameters obtained for the Ca-ATPase under these different experimental conditions indicates that the phosphorylation of PLB acts primarily to increase the residual anisotropy; there are no significant changes in the amplitudes (i.e., g_1) or rates of domain motions (i.e., ϕ_1) within the Ca-ATPase (Table 2). Likewise, the rotational correlation times associated with overall rotational motion are not appreciably altered, suggesting that phosphorylation of PLB does not alter the average structure of individual domains or oligomeric interactions between Ca-ATPase polypeptide chains.

One can obtain an appreciation of the structural changes involving domain elements within the Ca-ATPase resulting from PLB phosphorylation through a consideration of the relationship between the residual anisotropy (r_∞) and the angle of the principal dipole (θ_c) of Er-ITC chromophores

bound to domain elements within the Ca-ATPase relative to the membrane normal (Table 2). If it is assumed that the motion of the erythrosin chromophores bound to the Ca-ATPase have cylindrical symmetry relative to the membrane normal (*35*, *37*, *38*), then

$$\frac{r_\infty}{r_o} = [^1/_2 \cos\theta_c\,(1 + \cos\theta_c)]^2 \qquad (4)$$

Thus, the apparent average value for θ_c changes by $9 \pm 4°$ from $58 \pm 2°$ to $49 \pm 3°$ relative to the membrane normal upon phosphorylation of PLB, if one assumes that the orientations of both Er-ITC probes relative to the membrane normal are similar and move in the same direction relative to the membrane normal upon PLB phosphorylation. Since individual domain elements within the Ca-ATPase have been suggested to contain both cytoplasmic and transmembrane portions of the Ca-ATPase (*22*), these results suggest that the modulation of the spatial arrangement of domain elements can couple structural elements within the cytoplasmic region of the Ca-ATPase, involved in nucleotide binding and utilization, to the transmembrane domain, which are involved in calcium binding and translocation (*41*). It should be noted that since Er-ITC labels two sites, the observed change in erythrosin orientation may underestimate the change in the average angle of individual domain elements relative to the membrane normal.

DISCUSSION

Summary of Results. Phosphorescence anisotropy decay measurements offer the potential to detect large-scale structural changes of integral membrane proteins in their native membrane environment, and have been instrumental in identifying dynamic structural changes involving the Ca-ATPase (*22*, *41*, *42*, *43*). To investigate mechanisms of PLB regulation of Ca-ATPase function, we have selectively modified the Ca-ATPase in native cardiac SR microsomes with the long-lived phosphorescent probe Er-ITC, permitting measurements of large-scale global conformational changes involving domain elements within the Ca-ATPase using FD phosphorescence spectroscopy. Using HPLC and ESI-MS, two major labeling sites involving Lys^{464} and Lys^{650} have been identified for Er-ITC covalently bound to the SERCA2a isoform of the Ca-ATPase expressed in cardiac SR membranes, which are present in approximately equal stoichiometries (Table 1). In contrast, Lys^{464} is selectively labeled by Er-ITC in the homologous SERCA1 isoform of the Ca-ATPase expressed in skeletal SR membranes (*16*). Thus, it is not possible to quantitatively compare the phosphorescence anisotropy decay of the Ca-ATPase expressed in cardiac and skeletal SR (Figure 3 and Table 2), as the observed differences are probably, in part, related to differences in the Er-ITC labeling sites in the SERCA1 and SERCA2a isoforms that would be expected to alter the average orientation of the erythrosin chromophore(s) relative to he principal axis of rotational motion for the Ca-ATPase (*37*). Rather, these measurements provide useful information regarding possible alterations in the domain structure of the SERCA2a isoform of the Ca-ATPase following PLB phosphorylation or calcium activation.

We report that phosphorylation of PLB results in a substantial increase in the residual anisotropy of Er-ITC covalently bound to the Ca-ATPase in cardiac SR (Figure 4), suggesting that large-scale domain reorientations accompany the increase in cooperativity between high-affinity calcium sites. In contrast, prior to PLB phosphorylation, calcium activation of the Ca-ATPase results in no substantial change in the dynamic structure of individual domains (Figure 3 and Table 2). The lack of a significant calcium effect on the amplitude of motion in cardiac SR is in marked contrast to earlier results in skeletal SR (*22*). However, the insensitivity of Er-ITC dynamics to calcium activation for the SERCA2a isoform of the Ca-ATPase expressed in cardiac SR is consistent with earlier suggestions of a direct structural interaction between the transmembrane and cytosolic domains of PLB and the Ca-ATPase (*9*, *44*−*47*), which might be expected to restrict the amplitude of motion of individual domain elements and thereby diminish the sensitivity of the rotational motion of domain elements in the Ca-ATPase to structural changes involving the stalk region of the Ca-ATPase. This latter interpretation is consistent with the diminished amplitude associated with domain motions for SERCA2a in cardiac SR relative to that observed for SERCA1 SR (Table 2). Thus, PLB phosphorylation and calcium activation modulate Ca-ATPase activity through distinct mechanisms.

Relationship to Previous Results. In agreement with previous observations (*14*, *21*, *48*, *49*), we also find that the time-dependent loss of anisotropy for Er-ITC bound to the Ca-ATPase in cardiac SR is substantially reduced relative to that observed in skeletal SR (Figure 3). However, our results are in contrast to previous time-resolved phosphorescence anisotropy measurements that reported a large decrease in the residual anisotropy (r_∞) of Er-ITC bound to the Ca-ATPase in native cardiac SR membranes upon PLB phosphorylation, which have been interpreted to represent a large-scale decrease in the average oligomeric size of the Ca-ATPase (*5*, *14*, *21*, *48*, *50*, *51*). Thus, a quantitative interpretation of individual anisotropy decays requires that one ensure that the phosphorescence anisotropy is reporting only rotational motion. Other trivial mechanisms that can also promote depolarization involving, for example, homotransfer between proximal Er-ITC probes can be minimized through the covalent attachment of substoichiometric amounts of Er-ITC that decrease the likelihood that Er-ITC chromophores will be located at proximal positions on Ca-ATPase polypeptide chains (*15*). For example, in the presence of stoichiometric amounts of the phosphorescent probe eosin 5-maleimide bound at Lys^{430} within the erythrocyte anion exchange protein, band 3, observed changes in the residual phosphorescence anisotropy have been shown to be unrelated to any changes in oligomeric state, but rather primarily to reflect changes in homotransfer mechanisms involving the relative orientation or proximity of neighboring phosphorescent chromophores (*15*). These results argue against the simple interpretation of previous phosphorescence anisotropy decays for Er-ITC bound to the Ca-ATPase that were carried out at high labeling stoichiometries in terms of large populations of aggregated and rotationally immobile proteins (*14*). Rather, observed changes in the measured anisotropy of Er-ITC in earlier studies are more consistent with recently observed anisotropy changes for similar stoichiometries of fluorescein bound to SERCA2a that result from the reorientation of Ca-ATPase polypeptide chains with

respect to each other in a defined oligomeric state following the phosphorylation of PLB (*12*). In contrast, results reported in this paper emphasize the importance of using substoichiometric labeling conditions to ensure the absence of homotransfer between Er-ITC chromophores, so that observed changes in the time-dependent decay of anisotropy in terms of structural changes involving the Ca-ATPase could be unambiguously interpreted. The decreased rotational dynamics of the Ca-ATPase following the phosphorylation of PLB observed in this study are furthermore consistent with earlier ST-EPR measurements (*11*), which also found that decreases in the rotational dynamics of the Ca-ATPase occur upon PLB phosphorylation.

Mechanism of the Ca-ATPase and Functional Regulation by PLB. The Ca-ATPase has been suggested to belong to a large superfamily of hydrolases that are structurally typified by L-2-haloacid dehalogenase, and as is the case for other members of this superfamily, structural elements that are spatially distant within the primary sequence create a conserved active site (*52*). In analogy to numerous water-soluble protein kinases, the arrangement of predicted secondary structural motifs within the cytoplasmic portion of the Ca-ATPase suggests the presence of distinct domains associated with nucleotide binding and enzyme phosphorylation (*31*, *53*). These domains may correspond to the two cytoplasmic lobes resolved using image-enhanced electron microscopy (*46*). The mutations of numerous sites within these domains have been shown to interfere with nucleotide binding (*54*), and suggest topological constraints with respect to the arrangement of the primary sequences within the cytosolic portion of the Ca-ATPase. A cluster of short putative α-helices at the carboxyl-terminal end of the nucleotide binding domain is found to be juxtaposed with respect to the phosphorylation domain, and has been proposed to form a hinge that mediates changes in domain interactions during catalysis (*53*, *55*, *56*). Kinetic measurements of the rate constants associated with steps in the reaction cycle indicate that active calcium transport is coupled to ATP hydrolysis by means of the mutual destabilization between high-affinity calcium binding within transmembrane helices and the formation of a phosphoanhydride intermediate at Asp^{351} in the phosphorylation domain (*40*). This coupling has been suggested to involve a rigid structural linkage between the M4 transmembrane helix (Tyr^{294}−Thr^{316}), which contains at least one calcium ligand, and the phosphorylation domain through the connecting S4 stalk sequence (Thr^{317}−Lys^{329}).

The structural coupling between PLB and the Ca-ATPase in cardiac SR membranes may involve direct contact interactions in both the cytoplasmic and transmembrane domains. The porcine cardiac, SERCA2a, isoform of the Ca-ATPase contains a sequence near the nucleotide binding cleft, i.e., $KDDKPVK^{402}$, that is required for the functional interaction between PLB and the Ca-ATPase (*3*, *9*), suggesting that these residues may comprise a critical binding region. The homologous SERCA1 isoform of rabbit skeletal muscle has a similar sequence, $KNDKPIR^{402}$, and when coreconstituted with PLB is similarly regulated by changes in the extent of phosphorylation of PLB. While specific binding sites within either the Ca-ATPase or PLB transmembrane sequences have not been identified, the coexpression of the transmembrane sequence, alone, of PLB with the Ca-ATPase has been shown to inhibit transport activity at sub-micromolar calcium concentrations (*57*). Thus, one possible mechanism of regulation of Ca-ATPase function by PLB may involve the modulation of the long-range structural coupling between the high-affinity calcium binding sites located within the transmembrane helices and the spatially distant nucleotide binding site(s) located within the cytoplasmic portion of the Ca-ATPase. Consistent with this hypothesis, dephosphorylated PLB has been shown to modulate the calcium activation of the Ca-ATPase, resulting in reduced transport activity at sub-micromolar calcium concentrations as a result of decreased levels of phosphoenzyme intermediate (*58*). These results suggest that PLB functions to diminish the efficiency of the phosphoryl transfer reaction from ATP bound to the nucleotide binding domain to form the phosphoanhydride linkage to Asp^{351} in the phosphorylation domain. Consistent with this interpretation, our results indicate that PLB functions to modify the relative orientation of the nucleotide binding and phosphorylation domain elements with respect to one another (Figure 4 and Table 2), such that these domains move closer together following PLB phosphorylation to promote phosphoenzyme formation.

Conclusions and Future Directions. We have shown that phosphorylation of PLB by PKA functions to modify the relative orientation of domain elements within individual Ca-ATPase polypeptide chains. However, calcium activation and PLB phosphorylation are distinct processes that result in different structural changes to the Ca-ATPase. These measurements suggest that PLB functions as an allosteric modulator of Ca-ATPase function, whereby dephosphorylated PLB reduces the efficiency of phosphoryl transfer from ATP bound in the nucleotide binding domain to form the phosphoenzyme intermediate at Asp^{351} in the phosphorylation domain. Future studies should develop labeling methods for the specific covalent attachment of Er-ITC or other long-lived optical probes to defined sites in the SERCA2a isoform of the Ca-ATPase, permitting an assessment of how structural changes involving individual domain elements of the Ca-ATPase affect function and are modified by PLB association and phosphorylation.

ACKNOWLEDGMENT

We thank Todd D. Williams and Homigol Biesiada of the Kansas University Mass Spectrometry Laboratory for their efforts in peptide separation and ESI spectral acquisition and Diana J. Bigelow for insightful discussions.

REFERENCES

1. Tada, M., Kirchberger, M. A., and Katz, A. M. (1975) *J. Biol. Chem. 250*, 2640−2647.
2. Inui, M., Chamberlain, B. H., Saito, A., and Fleischer, S. (1986) *J. Biol. Chem. 261*, 1794−1800.
3. James, P., Inui, M., Tada, M., Chiesi, M., and Carafoli, E. (1989) *Nature 342*, 90−92.
4. Wegener, A. D., Simmerman, H. K., Lindemann, J. P., and Jones, L. R. (1989) *J. Biol. Chem. 264*, 11468−11474.
5. Simmerman, H. K., and Jones, L. R. (1998) *Physiol. Rev. 78*, 921−947.
6. Lindemann, J. P., Jones, L. R., Hathaway, D. R., Henry, B. G., and Watanabe, A. M. (1983) *J. Biol. Chem. 258*, 464−471.
7. Stokes, D. L. (1997) *Curr. Opin. Struct. Biol. 8*, 550−556.
8. Toyofuku, T., Kurzydlowski, K., Tada, M., and MacLennan, D. H. (1993) *J. Biol. Chem. 268*, 2809−2815.

9. Toyofuku, T., Kurzydlowski, K., Tada, M., and MacLennan, D. H. (1994) *J. Biol. Chem. 269*, 22929−22932.
10. Negash, S., Sun, H., Yao, Q., Goh, S., Bigelow, D., and Squier, T. (1998) *Ann. N.Y. Acad. Sci. 853*, 288−291.
11. Negash, S., Chen, L. T., Bigelow, D. J., and Squier, T. C. (1996) *Biochemistry 35*, 11247−11259.
12. Chen, L., Yao, Q., Brungardt, K., Squier, T., and Bigelow, D. (1998) *Ann. N.Y. Acad. Sci. 853*, 264−266.
13. Chamberlain, B. K., Berenski, C. J., Jung, C. Y., and Fleischer, S. (1983) *J. Biol. Chem. 258*, 11997−12001.
14. Voss, J., Jones, L. R., and Thomas, D. D. (1994) *Biophys. J. 67*, 190−196.
15. Blackman, S. M., Piston, D. W., and Beth, A. H. (1998) *Biophys. J. 75*, 1117−1130.
16. Huang, S., Negash, S., and Squier, T. C. (1998) *Biochemistry 37*, 6949−6957.
17. Ferrington, D. A., Moewe, P. L., Yao, Q., and Bigelow, D. J. (1998) *Biophys. J. 74*, 356a.
18. Lanzetta, P. A., Alvarez, L. J., Reinach, P. S., and Candia, O. A. (1979) *Anal. Biochem. 100*, 95−97.
19. Swenson, C. A., and Fredricksen, R. S. (1992) *Biochemistry 31*, 3420−3429.
20. Schaffner, W., and Weissmann, C. (1973) *Anal. Biochem. 56*, 502−514.
21. Birmachu, W., Voss, J. C., Louis, C. F., and Thomas, D. D. (1993) *Biochemistry 32*, 9445−9453.
22. Huang, S., and Squier, T. C. (1998) *Biochemistry 37*, 18064−18073.
23. Eads, T. M., Thomas, D. D., and Austin, R. H. (1984) *J. Mol. Biol. 179*, 55−81.
24. Laemmli, U. K. (1970) *Nature 227*, 680−685.
25. Eggermont, J. A., Wuytack, F., De Jaegere, S., Nelles, L., and Casteels, R. (1989) *Biochem. J. 260*, 757−761.
26. Weber, G. (1981) *J. Phys. Chem. 85*, 949−953.
27. Lakowicz, J. R., Cherek, H., and Maliwal, B. P. (1985) *Biochemistry 24*, 376−383.
28. Beechem, J., Gratton, E., Ameloot, M., Knutson, J. R., and Brand, L. (1991) in *Topics in Fluorescence Spectroscopy* (Lakowicz, J. R., Ed.) Vol. 2, pp 241−306, Plenum Press, New York.
29. Johnson, M. L., and Faunt, L. M. (1992) *Methods Enzymol. 210*, 1−37.
30. Haugland, R. (1996) *Handbook of Fluorescent Probes and Research Chemicals*, Molecular Probes, Inc., Eugene, OR.
31. MacLennan, D. H., Brandl, C. J., Korczak, B., and Green, N. M. (1985) *Nature 316*, 696−700.
32. Murphy, A. J. (1988) *Biochim. Biophys. Acta 946*, 57−65.
33. Mignaco, J. A., Lupi, O. H., Santos, F. T., Barrabin, H., and Scofano, H. M. (1996) *Biochemistry 35*, 3886−3891.
34. Lakowicz, J. R. (1983) *Principles of Fluorescence Spectroscopy*, Plenum Publishing Corp., New York.
35. Kinosita, K., Ishiwata, S., Yoshimura, H., Asai, H., and Ikegami, A. (1984) *Biochemistry 23*, 5963−5975.
36. Birmachu, W., and Thomas, D. D. (1990) *Biochemistry 29*, 3904−3914.
37. Fajer, P., Knowles, P. F., and Marsh, D. (1989) *Biochemistry 28*, 5634−5643.
38. Cherry, R. J. (1992) in *The Structure of Biological Membranes* (Yeagle, P., Ed.) pp 507−537, CRC Press, Boca Raton, FL.
39. Esmann, M., Hideg, K., and Marsh, D. (1994) *Biochemistry 33*, 3693−3697.
40. Inesi, G. (1994) *Biophys. J. 66*, 554−560.
41. Cornea, R. L., and Thomas, D. D. (1994) *Biochemistry 33*, 2912−2920.
42. Hunter, G. W., Negash, S., and Squier, T. C. (1999) *Biochemistry 38*, 1356−1364.
43. Hunter, G. W., Bigelow, D. J., and Squier, T. C. (1999) *Biochemistry* (in press).
44. Kumura, Y., Kurzydlowski, K., Tada, M., and MacLennan, D. H. (1997) *J. Biol. Chem. 272*, 15061−15064.
45. MacLennan, D. H., Kimura, Y., and Toyofuku, T. (1998) *Ann. N.Y. Acad. Sci. 853*, 31−42.
46. Ogawa, H., Stokes, D. L., Sasabe, H., and Toyoshima, C. (1998) *Biophys. J. 75*, 41−52.
47. Kühlbrandt, W., Auer, M., and Scarborough, G. A. (1998) *Curr. Opin. Struct. Biol. 8*, 510−516.
48. Voss, J. C., Mahaney, J. E., Jones, L. R., and Thomas, D. D. (1995) *Biophys. J. 68*, 1787−1795.
49. Kutchai, H., Geddis, L. M., Jones, L. R., and Thomas, D. D. (1998) *Biochemistry 37*, 2410−2421.
50. Karon, B. S., Geddis, L. M., Kutchai, H., and Thomas, D. D. (1995) *Biophys. J. 68*, 936−945.
51. Thomas, D. D., Reddy, L. G., Karim, C. B., Cornea, R., Autry, J. M., Jones, L. R., and Stamm, J. (1998) *Ann. N.Y. Acad. Sci. 853*, 186−194.
52. Aravind, L., Galperin, M. Y., and Koonin, E. V. (1998) *Trends Biochem. Sci. 23*, 127−129.
53. MacLennan, D. H., Rice, W. J., and Green, N. M. (1997) *J. Biol. Chem. 272*, 28815−28818.
54. MacLennan, D. H. (1990) *Biophys. J. 58*, 1355−1365.
55. Taylor, W. R., and Green, N. M. (1989) *Eur. J. Biochem. 179*, 241−248.
56. Møller, J. V., Juul, B., and le Maire, M. (1996) *Biochim. Biophys. Acta 1286*, 1−51.
57. Kimura, Y., Kurzydlowski, K., Tada, M., and MacLennan, D. H. (1996) *J. Biol. Chem. 271*, 21726−21731.
58. Cantilina, T., Sagara, Y., Inesi, G., and Jones, L. R. (1993) *J. Biol. Chem. 268*, 17018−17025.
59. Anderson, R. L. (1987) *Practical Statistics for Analytical Chemists*, Van Nostrand Reinhold, New York.

BI990599J